ADVANCED HEALTHCARE MATERIALS
www.advhealthmat.de

Multifunctional Skin-Like Electronics for Quantitative, Clinical Monitoring of Cutaneous Wound Healing

Yoshiaki Hattori, Leo Falgout, Woosik Lee, Sung-Young Jung, Emily Poon, Jung Woo Lee, Ilyoun Na, Amelia Geisler, Divya Sadhwani, Yihui Zhang, Yewang Su, Xiaoqi Wang, Zhuangjian Liu, Jing Xia, Huanyu Cheng, R. Chad Webb, Andrew P. Bonifas, Philip Won, Jae-Woong Jeong, Kyung-In Jang, Young Min Song, Beatrice Nardone, Michael Nodzenski, Jonathan A. Fan, Yonggang Huang, Dennis P. West, Amy S. Paller, Murad Alam, Woon-Hong Yeo, and John A. Rogers**

Non-invasive, biomedical devices have the potential to provide important, quantitative data for the assessment of skin diseases and wound healing. Traditional methods either rely on qualitative visual and tactile judgments of a professional and/or data obtained using instrumentation with forms that do not readily allow intimate integration with sensitive skin near a wound site. Here, an electronic sensor platform that can softly and reversibly laminate perilesionally at wounds to provide highly accurate, quantitative data of relevance to the management of surgical wound healing is reported. Clinical studies on patients using thermal sensors and actuators in fractal layouts provide precise time-dependent mapping of temperature and thermal conductivity of the skin near the wounds. Analytical and simulation results establish the fundamentals of the sensing modalities, the mechanics of the system, and strategies for optimized design. The use of this type of "epidermal" electronics system in a realistic clinical setting with human subjects establishes a set of practical procedures in disinfection, reuse, and protocols for quantitative measurement. The results have the potential to address important unmet needs in chronic wound management.

1. Introduction

Quantitative monitoring of wound healing, a dynamic interactive biological process involving blood cells, extracellular matrix, and parenchymal cells, is of great interest in biomedical research and clinical practice. The most comprehensive assessment is based on histological evaluation of tissue morphologic change,[1,2] but this procedure is invasive and does not provide a means for continuous evaluation over time. Visual inspection by digital photography[1,3,4] overcomes these limitations, but interpretation is inherently subjective and the imaging often yields inconsistent information due to variations in lighting, focus, and angle. Quantitative imaging

Dr. Y. Hattori, L. Falgout, Dr. J. W. Lee, R. C. Webb, Dr. A. P. Bonifas, P. Won, Dr. J.-W. Jeong, Dr. K.-I. Jang, Dr. J. A. Fan
Department of Materials Science and Engineering
and Frederick Seitz Materials Research Laboratory
University of Illinois at Urbana-Champaign
Urbana, IL 61801, USA

W. Lee
Department of Electrical Engineering
University of Illinois at Urbana-Champaign
Urbana, IL 61801, USA

S.-Y. Jung
Department of Mechanical Engineering
Pohang University of Science and Technology
Pohang 790–784, Republic of Korea

Dr. E. Poon, A. Geisler, D. Sadhwani, Dr. X. Wang, Dr. B. Nardone, M. Nodzenski, Dr. D. P. West, Dr. A. S. Paller, Dr. M. Alam
Department of Dermatology
Feinberg School of Medicine
Northwestern University
Chicago, IL 60611, USA

I. Na
Department of Chemical Engineering
Pohang University of Science and Technology
Pohang 790–784, Republic of Korea

Dr. Y. Zhang, Dr. Y. Su, J. Xia, H. Cheng, Prof. Y. Huang
Department of Civil and Environmental Engineering
Department of Mechanical Engineering
Center for Engineering and Health
and Skin Disease Research Center
Northwestern University
Evanston, IL 60208, USA

Dr. Y. Zhang, Dr. Y. Su, J. Xia
Center for Mechanics and Materials
Tsinghua University
Beijing 100084, China

Prof. Z. Liu
Institute of High Performance Computing
A*star, 1 Fusionopolis Way, #16–16, Connexis 138632, Singapore

Prof. Y. M. Song
Department of Electronic Engineering
Pusan National University
Busan 609–735, Republic of Korea

Prof. W.-H. Yeo
Department of Mechanical and Nuclear Engineering
and Institute for Engineering and Medicine
Virginia Commonwealth University
Richmond, VA 23284, USA
E-mail: whyeo@vcu.edu

Prof. J. A. Rogers
Department of Materials Science and Engineering
Beckman Institute for Advanced Science and Technology
and Frederick Seitz Materials Research Laboratory
University of Illinois at Urbana-Champaign
Urbana, IL 61801, USA
E-mail: jrogers@illinois.edu

DOI: 10.1002/adhm.201400073

methods via confocal laser scanning microscopy or spectroscopy can reveal microscopic level changes in the morphology of the epidermis and dermis.[4,5] These methods, however, require patient immobilization during the testing. Also, the required sophisticated optical systems are high in cost and require trained personnel for evaluation. Recent work on simple, portable, point-of-care devices[1,6] for optical sectioning and topical determination of wound healing phases suggests promise, although their use is ultimately limited by qualitative visual evaluation. In wound healing, calor is a primary indicator of inflammation and possible infection.[1,7,8] Hydration is another factor that affects wound healing.[9] Thus, monitoring of skin temperature and thermal conductivity (hydration), along with numerous other potential markers such as bacterial load, cytokine release, DNA, enzymes, hormones, pH, oxygen, and transepidermal water loss,[1] can provide important clinical information.

Practical biomedical devices, capable of non-invasive, quantitative, and multifunctional measurements of the healing process, are needed to complement optical and other techniques. In this communication, we introduce a skin-like electronics system capable of precise and real-time monitoring of cutaneous wound healing in a clinical setting. These devices represent a type of epidermal electronics system (EES),[10] which adopts the soft mechanical texture of the epidermis to allow conformal lamination and reversible bonding to the epidermis via van der Waals interactions alone.[11–13] The result is a natural, non-irritating and high-quality interface to the skin that does not constrain natural motions or induce any discomfort.[12] EES can be designed in biocompatible, waterproof forms that are easily disinfected for clinical applications, enabling re-use. The sensors demonstrated here use microscale, metal traces in fractal layouts on soft, elastomeric membranes, capable of measurement and mapping of skin temperature with an accuracy comparable to that of a high-end infrared (IR) camera, with the additional capabilities of recording thermal conductivity and delivering precise levels of heating.

In wound healing monitoring, an EES records time-dynamic temperature and thermal conductivity of the skin tissue. Mapping of skin temperature is important because it captures the "inflammation" phase of the healing process, related to increased blood flow to the wound.[14,15] Thermal conductivity correlates strongly to hydration state, which is another important aspect of wound care, and can serve as an early sign of the emergence of local edema.[16–18] From a practical standpoint, thermal conductivity can also serve as a sensitive indicator of quality of contact between the device and the wound, allowing the healthcare professional to assess proper mounting on the skin. Three dimensional mechanical and thermal simulations of this type of EES on human skin, through the finite element method (FEM) and the finite volume method (FVM), respectively, capture the underlying physics of this contact, as well as the mechanisms for physiological sensing. The results establish critical design criteria for clinical applications.

2. Results

2.1. Device Design and Mechanics Modeling

Figure 1a presents a schematic view of a multifunctional EES. The device uses a multilayer construct that consists of metal traces with fractal geometries (Peano curve motif) in an interconnected collection of ultrathin filamentary serpentine (FS) traces in an open mesh configuration. Contact pads provide connection points to external data acquisition hardware. The fractal configuration offers superior elastic stretchability compared to conventional meandering structures[19] and, in the context reported here, enables precise thermal measurements in ways that are largely unaffected by mechanical strains associated with mounting onto the complex cutaneous wound shapes. FEM analysis (Note 1 and Figure S1, Supporting Information) illustrates quantitatively the elastic properties of the fractal geometry chosen for present purposes, with a comparison to other fractal options, as well as conventional designs such as regular curves and serpentines. The sensors are integrated onto thin silicone membranes (dyed black to facilitate control measurements of temperature with an IR camera) by the techniques of transfer printing, and subsequently coated with an encapsulating layer of silicone.[20] The resulting EES offers effective elastic moduli (22.1 kPa, measured by DMA Q800, TA instruments, USA) that are significantly lower than those of the epidermis (100–150 kPa). Figure 1b–e shows the response upon 30% uniaxial stretching (Figure 1b), multimodal folding (Figure 1c), biaxial stretching and twisting (Figure 1d), and 720° twisting (Figure 1e).

The device fabrication follows procedures described briefly in the Methods section, with details in Supplementary Note 2 and Figure S2 and S3 (Supporting Information). The process exploits conventional microfabrication techniques to form electronic structures on a silicon wafer coated with a sacrificial polymer, as a temporary carrier substrate. The conducting elements use 3-μm-thick copper (Cu) traces deposited by electron-beam evaporation. Layers of polyimide (PI; 1.2 μm in thickness; Sigma-Aldrich, USA) above and below place the Cu fractal (width: 35 μm) and FS traces (width: 50 μm) at the neutral mechanical plane (NMP) to minimize the bending strains. Water-soluble tapes can be used to retrieve the electronic structures from the carrying wafer and to transfer them to a silicone membrane (500 μm in thickness, ≈20 kPa in modulus; Ecoflex, Smooth-On, USA; Figure 1a).[12] A 5-μm-thick layer of silicone spin cast on top of the device encapsulates the EES to provide a water-proof surface capable of sterilization for use in clinical studies with human patients.[20]

Figure 1f (top view) and Figure 1g (tilted view) show microscale X-ray coherent tomography images (microXCT, Xradia, USA) of such a device.[21] The fractal construct accommodates levels of mechanical strain upon biaxial, radial stretching that exceed maximum values (≈30%) typically experienced in the skin.[10] Details of the microXCT imaging process appear in the Supplementary Note 3 (Supporting Information). FEM analysis (details in Figure S4, Supporting Information) and experimental studies with microXCT (Figure 1h) reveal that the fractal systems can be stretched by ≈15% and ≈30% with only 0.25% and 0.85% maximum principal strain in the Cu (elastic strain of Cu: 0.3%; fracture strain of Cu: 5%),[22–24] respectively. The results (Figure 1h) suggest ability to ensure consistent, reproducible device function, and operation at and beyond levels of deformation that can be tolerated by the skin (10%–20%).[11,20]

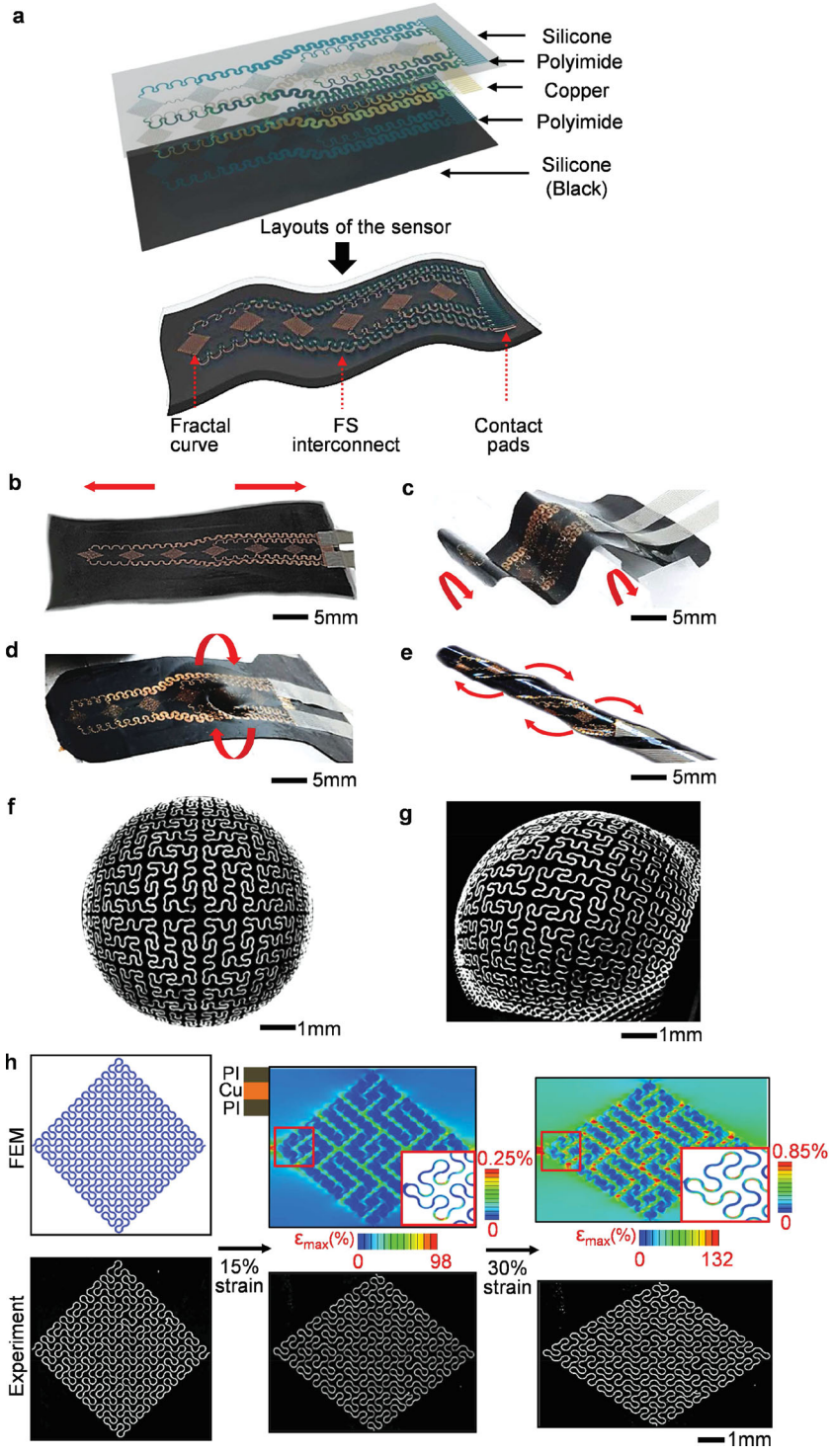

Figure 1. Device design and mechanics modeling. a) Schematic illustration of an EES. b) Image of an device under c) uniaxial stretching, multimodal folding and d) biaxial stretching and twisting and 720° twisting (e). f) Top view and tilted view g) micro-XCT images of the device in (d). h) FEM analysis and experimental study of a fractal construct under uniaxial stretching; FEM (top) and experiment (bottom). The inset in the middle illustrates the neutral mechanical plane (NMP) of the metal with polyimide (PI) encapsulation.

2.2. Multifunctional Characteristics

Figure 2 summarizes the hardware and capabilities of an integrated collection of components, consisting of data acquisition systems and an EES with an array of sensors and actuators, configured for multipoint mapping of temperature, and thermal conductivity. The devices include an EES (wound compatible device), a current source (6221, Keithley Instruments, USA), a lock-in amplifier (SR830, Stanford Research Systems, USA), a multiplexer (FixYourBoard.com, U802, USA), and a laptop (Figure 2a). A thin, flexible ribbon cable (HST-9805-210, Elform, USA) connects the array of six sensors/actuators in the EES to a multiplexer that enables sequential operation for spatial recording of temperature and thermal conductivity. The measurement uses a four-point-probe technique for determining voltage drop in the sensors[19] upon changes in temperature or mechanical strain (Figure S5, Supporting Information). Figure 2b lists representative operating parameters for the lock-in amplifier during thermal conductivity and temperature measurements. Custom software presents a user-friendly interface that automatically calculates relevant parameters from voltages recorded through a GPIB cable interface (NI GPIB-USB-HS, National Instruments Corp., USA) to the computer. Changes in electrical resistance of the fractal constructs allow determination of changes in temperature, through a calibration curve (Figure 2c) established using data from an IR camera (precision <50 mK, A655SC, FLIR, USA) and a precisely controlled hot plate (details in Supplementary Note 4, Supporting Information). The resistance is calculated from voltage drops measured across the sensors. The precision of an EES is ≈50 mK, determined by limitations in the analogue-to-digital converter. Absolute accuracy in clinical testing is ≈200 mK, limited by the parameters of the constant current source used in the system.

Evaluation of thermal conductivity uses an alternating current (AC) method adapted from techniques previously used in other contexts, known as the 3 omega (3ω) method.[25] Here, an AC current applied to the fractal structures induces both heating and changes in resistance that, in turn, influence the heating levels. This nonlinear coupling leads to a voltage output at the third harmonic of the AC drive. The magnitude of

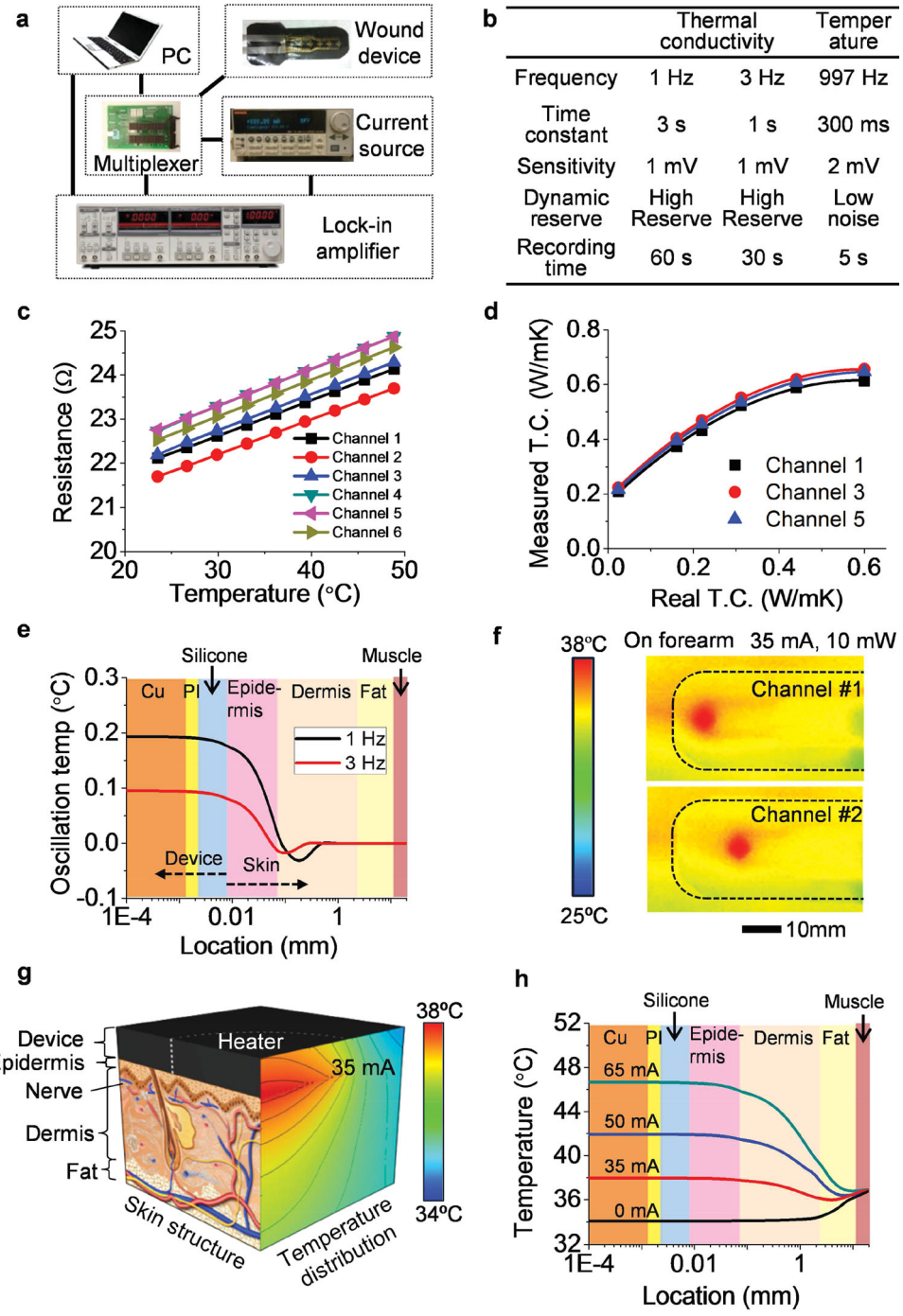

Figure 2. Multifunctional characteristics. a) Data acquisition system. b) Parameters of the lock-in amplifier for measurement of temperature and thermal conductivity. c) Electrical resistance of six sensors in an EES, as a function of surface temperature. d) Measurement of thermal conductivity by an EES. e) Simulation of the oscillating temperature distribution induced in the skin by the EES. f) IR thermography during Joule heating (35 mA) using one of the sensors in the EES as a micro-heater. g) Simulation of the rise in temperature on the surface of the device upon Joule heating (35 mA). h) Simulation of the rise in temperature on the skin tissue on the device surface upon Joule heating.

this signal is influenced by the thermal conductivity of the contacting material, that is, the human skin. Details of the measurement schemes and calibration procedures appear in Supplementary Note 5 (Supporting Information). The frequency dependence of the 3ω voltage signals for operation in air and the associated amplitude of the temperature oscillations are shown in Supplementary Figures S7 and S8 (Supporting Information), respectively. 3ω voltages measured at two different AC frequencies can be used with a simple analytical expression to determine the thermal conductivity:[25]

$$\lambda = \frac{R_0 I_{rms}^3 \ln(f_H/f_L)dR}{4l\pi(V_{3\omega L} - V_{3\omega H})dT} \quad (1)$$

where R_0 is the nominal resistance of the sensor, I_{rms} is the applied root-mean-square (RMS) current at 1ω, f_H is a selected higher frequency, f_L is a lower frequency, l is the length of the sensor, and $V_{3\omega}$ is the measured RMS voltage at 3ω (L and H denote lower and higher, respectively), and dR/dT is resistance change as a function of temperature. Calibration using samples with known values of thermal conductivity is required to account for various aspects of the device structure and non-linearity in the response. The two frequencies chosen for the measurement offer the best compromise of skin characterization and reduced time for clinical measurement on patients.

Figure 2d presents the calibrated relationship between the thermal conductivity measured using an EES for six examples where the conductivity is known (air, concentrations of 0, 25, 50, 75, and 100% ethanol in water).[26] The measurements involve probing to effective depths that depend on various details, including the frequency, as illustrated in results of Figure 2e obtained by numerical analysis for the case of a simplified model of human skin. Here, a quasi-steady-state form of the heat conduction equation can be solved at the operating frequency by the finite volume method (FVM) with a 2D approximation[27] (details in Supplementary Note 6 and Table S1, Supporting Information). The amplitude of temperature oscillations at the fractal sensor (Figure 2e) decreases sharply from the EES and its point of skin contact, and later converges in the dermis layer. The characteristic distribution of these curves follows expected patterns as reported earlier.[28] For frequencies used in our clinical studies (i.e., $V_{3\omega L}$ = 1 Hz and $V_{3\omega H}$ = 3 Hz), the measured thermal conductivity is influenced by properties of both the epidermis and dermis.

We note that the heating functionality needed for assessment of thermal conductivity might be advantageous separately in a therapeutic mode. The steady-state temperature distribution associated with Joule heating is important in this context. Modeling of the well-known Pennes bioheat transfer equation, with FVM and 2D approximations (Supplementary Note 7, Supporting Information), yields results shown in Figure 2g. Figure 2h presents calculated temperature distributions for various input currents, where increased temperature can be observed down to the dermis layer. Applied currents (35, 50, and 65 mA) yield peak temperatures of 38, 42, and 46 °C, respectively. These temperatures can be measured and controlled accurately by using the heaters simultaneously as temperature sensors. This study indicates, therefore, some potential of an EES for therapeutic use since local heating is known to promote healing of chronic wounds[29,30] and has been used in hyperthermia treatment of some skin cancers.[29,31–33]

2.3. Device Characterization

The mechanical, thermal, and measurement properties are critical to the operation of the devices. For example, mechanical deformations can induce strains in the sensors, with the potential to change their resistances in ways that might confound temperature and thermal conductivity measurements. This effect can have practical importance, simply because uniaxial stretching and multimodal bending can occur in the process of applying and removing the device from the skin. These mechanical deformations may also cause slight, permanent changes in the resistance of the sensors by plastic deformation. Fractal choices in layout, guided by FEM analysis of the mechanics, can minimize such effects.[19] **Figure 3**a shows the contribution of cyclic uniaxial loading to a maximum elongation of 15%. The device is first stretched to 15% and then released back to 0% (details in Supplementary Note 8, Supporting Information). The measurements reveal elastic elongation and release response without hysteresis in the stress–strain curve (Figure 3a). The resistance change of 0.025% at 15% elongation changes the apparent temperature reading by only 0.05 °C. Figure 3b shows that temperature changes due to bending are negligible (temperature shift: <0.01 °C) for bending radii between 15 and 45 mm. Results indicated relatively small effects of deformation on thermal measurement; further reductions are possible with refined device designs.

Direct and simultaneous comparison of temperature recordings using an EES and IR camera supports the accuracy and reproducibility of measurements of temperature, as outlined in Supplementary Note 9 (Supporting Information). Figure 3c presents an IR thermogram of a forearm with an EES laminated on the skin, revealing increased temperature in locations of arteries. Figure 3d compares temperature distributions on the skin measured using an EES with that from an IR camera. Due to thermal convection on the air-exposed surface of the device, the skin temperature from the EES is slightly higher than (0.6 ± 0.4 °C) that from the IR thermogram. The shifted IR thermogram temperature matches well with EES data. The thermal conductivity must be assessed independently, as this quantity cannot be determined with the IR camera. Figure 3e presents a measurement on the forearm with a wet piece of paper under sensor #3. The locally increased thermal conductivity results in an expected increased thermal conductivity reading from this sensor. Other sensors yield values that are typical epidermis thermal conductivity values (0.1–0.3 W mK^{-1}) (Figure 3f).

For practical application in the clinic, these measurement capabilities must not be altered by standard procedures for disinfection of devices that are placed on the skin, such as rubbing the application area with isopropyl alcohol antiseptic.[34–36] Per protocol, each EES was prepared in this way immediately prior to use (details in Supplementary Note 10 and Figure S19, Supporting Information). Device functions were examined after multiple cleaning steps, by recording thermal conductivity values at three different conditions. The graph in Figure 3g presents measurement results after cleaning procedures with air exposure, 50% ethanol/water mixture, and acrylic board (OPTIX, Plaskolite, USA) over multiple cycles of cleaning. Values in all cases are consistent with the known thermal conductivity values, indicated by the straight lines. Related evaluations on the skin can be accomplished by examining repeatability in measurements performed at a single anatomic site. Figure 3h shows thermal conductivity values from 20 measurements. Results show good repeatability, with a precision of

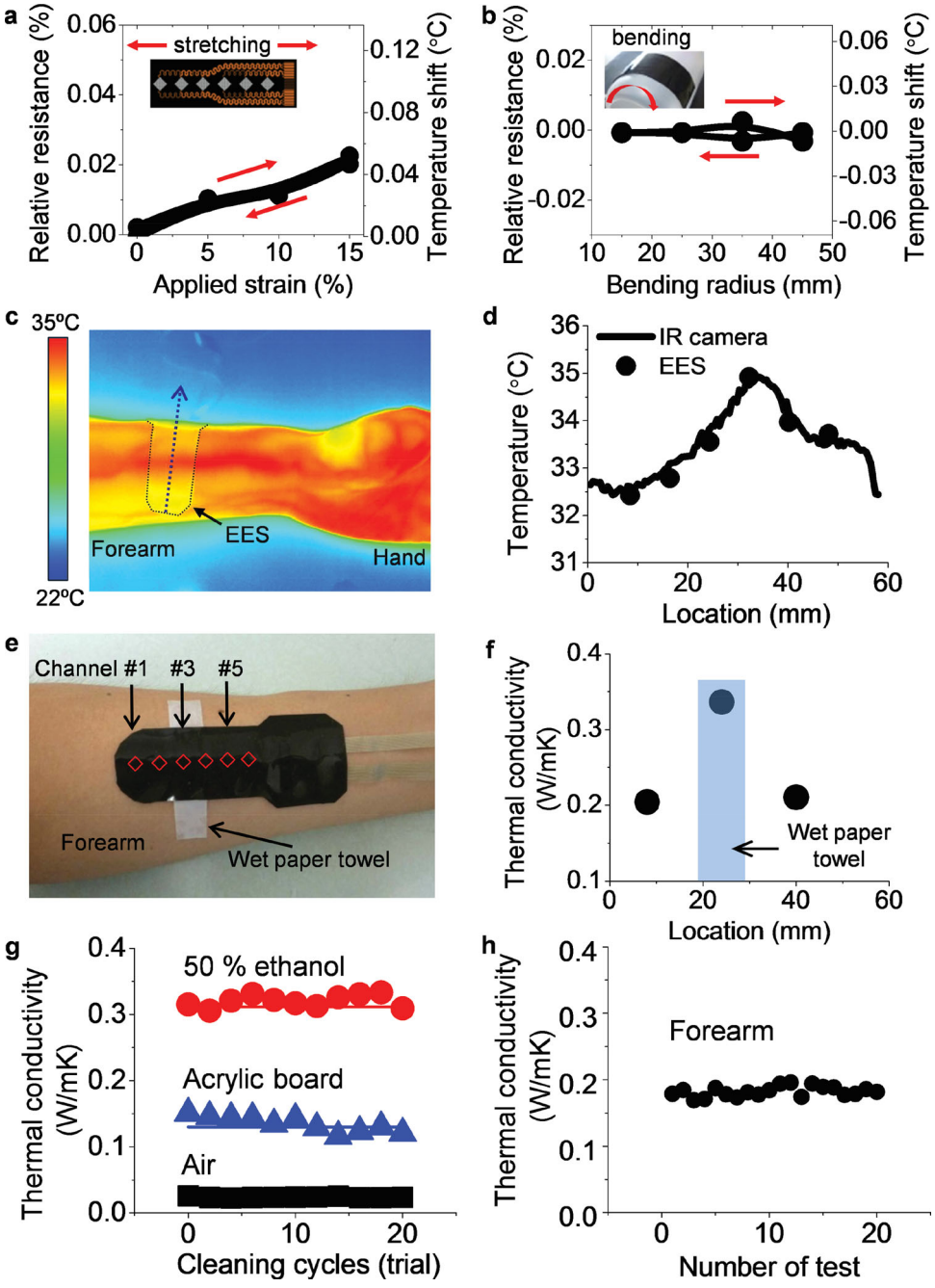

Figure 3. Device characterization. a) Effect of mechanical stretching on the measured temperature. b) Effect of bending on the measured temperature. c) IR thermogram of the forearm with an EES mounted. d) Temperature distribution on the skin measured by the IR camera and the EES along blue dotted line shown in (c). The horizontal axis shows the distance from the top of the heater. e) EES mounted on the forearm with a wet paper towel that covers sensor #3. f) Distribution of measured thermal conductivity of the skin. The value from sensor #3 shows a clear, expected difference from the other sensors. g) Thermal conductivity of air, 50% ethanol, and acrylic sheet measured after multiple cycles of cleaning. The straight lines in the graph show the actual values. h) Thermal conductivity measured on the forearm 20 times on one individual.

≈4%. This result is important because it suggests that the soft construction of the EES allows consistent conformal contact with the surface of the skin, consistent with previous observations in other contexts.[18] The interfacial contact adhesion between the EES and the skin is ≈0.5 N m^{-1} as measured in mechanical peel tests using a force gauge (Mark-10, USA).[12]

2.4. Use of EES on Human Subjects in a Clinical Setting

Adhesion and skin irritation of the EES versus conventional medical skin tape (3M, USA; major ingredient, acrylate polymer)[12] was determined by mounting on the forearm (**Figure 4**a–g). Observation of the skin by a digital contact

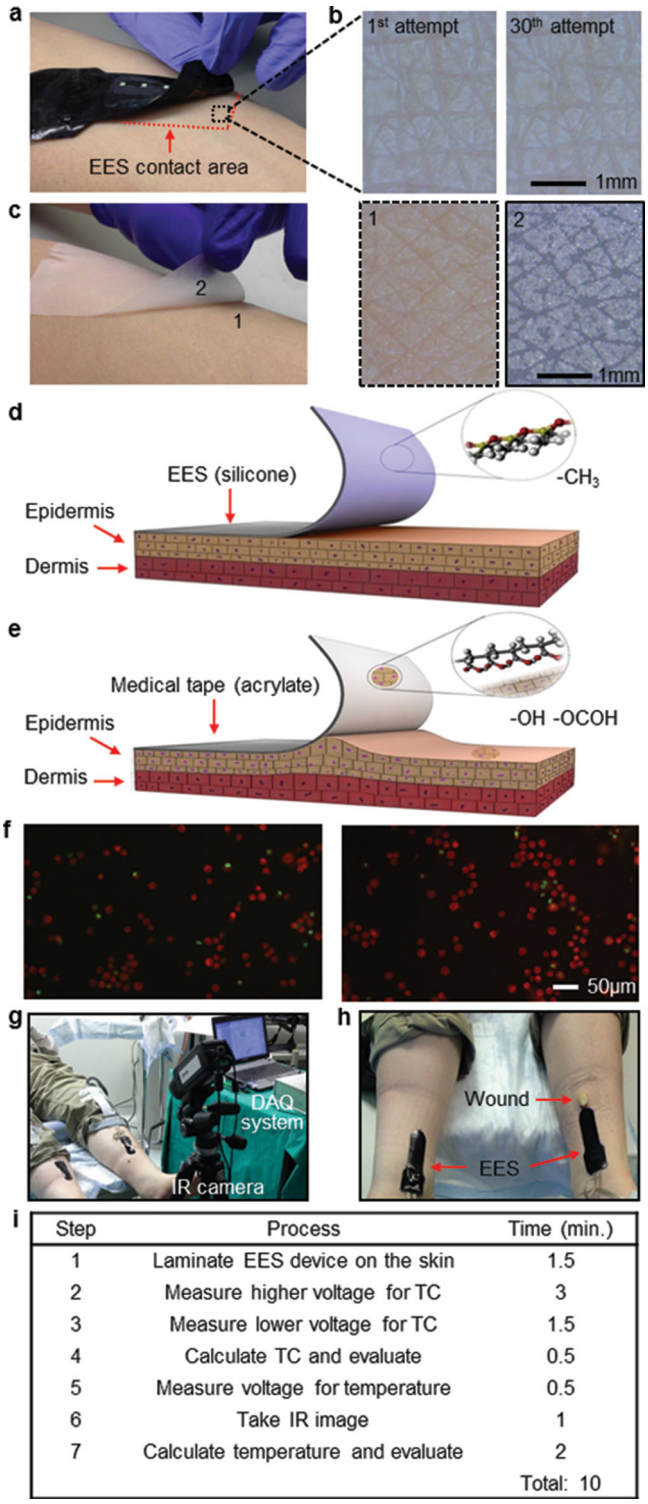

i

Step	Process	Time (min.)
1	Laminate EES device on the skin	1.5
2	Measure higher voltage for TC	3
3	Measure lower voltage for TC	1.5
4	Calculate TC and evaluate	0.5
5	Measure voltage for temperature	0.5
6	Take IR image	1
7	Calculate temperature and evaluate	2
		Total: 10

Figure 4. Use of an EES on human subjects in a clinical setting. a) EES laminated on the skin (forearm) after sterilization. b) Microscope images of the skin with 30 separate processes of mounting and removing an EES. c) Microscope image of the skin after the medical tape removal (1) and image of the tape surface (2). d) Illustration of the materials interface between the EES and skin e) Illustration of the medical tape and skin. f) Fluorescence images of viability of skin cells grown on an EES (left) and the results of control experiments on standard cell culture materials (right). Most of the cells on the EES remain viable ("red" cells). g) Clinical setting for wound monitoring in a typical exam room. h) EES laminated on wound and contralateral (control) sites. i) Assessment sequence and estimated time.

microscope (AM7013MT Dino-Lite, AnMo Electronics, USA) after mounting was used to assess skin irritation (erythema and scaling) qualitatively. Despite more than 30 episodes of mounting and removal on the same anatomic skin site, EES did not cause any clinical evidence of irritation (Figure 4a,b). In contrast, acrylate-based medical tape caused slight erythema upon removal (Figure 4c-1), likely due to partial exfoliation of the stratum corneum by the adhesive (Figure 4c-2). The silicone surface of the EES presents hydrophobic methyl groups; the acrylate tape presents hydrophilic hydroxyl groups (Figure 4d,e). The general, non-covalent interfaces of the EES offer sufficient adhesion for conformal contact (Figure 3h), similar to the adhesion of dry skin adhesives.[37–40] To further assess the potential impact of EES on keratinocyte (skin cell) viability, normal human keratinocytes were seeded onto the EES and viability was tested with a live/dead staining assay kit. Fluorescence microscopic images show that most cells cultured on the EES remain viable (stained as "red")[41–43] (Figure 4f).

Three subjects with incisional cutaneous wound sites participated in the studies (Figure 4g,h). Two devices were used: one in proximity to the surgical wound site and the other at the comparable area on the contralateral side as a control for evaluating time dynamic natural variations in body temperature. Optimization of the system construction and recording parameters enabled rapid, multi-point evaluation of temperature, and thermal conductivity, as well as comparison of the former results to those simultaneously obtained with an IR camera, with a total measurement time of only 10 minutes (Figure 4i). **Figure 5**a presents images at day 1, 3, 15, and 30 with the EES in intimate contact perilesionally to the cutaneous wound with comparison to IR thermography at a single time point (Figure 5b). Measurements from the contralateral site are in Figure S20 (Supporting Information). The EES for temperature and thermal conductivity recording incorporates six sensing components along an overall length of 45 mm. Figure 5c presents variations in temperature recorded by the six sensors, as shown by arrows (inset) from day 1 to 30. The normalized data (Figure 5c, right) reveal relative temperature differences adjacent to the wound site compared with normal skin. The sudden temperature rise on day 3, as indicated in the graph, captures the inflammation phase, which is thought to be due to increased blood flow and enzymatic reactions.[1,14,15,44] The control experiment (Figure 5d) on the contralateral site serves to establish the baseline temperature at a comparable location without a wound. Measurement of localized, tissue thermal conductivity with the same device enables assessment of conformal contact and skin hydration (Figure 5e).[18] On day 3, when the wound is considered to be in the inflammation phase, the corresponding thermal conductivity is slightly lower than at other time frames. To our knowledge, no previous studies have reported such variations in hydration, particularly near or on the hypersensitive wound tissue, during the healing process. Other works regarding hydration monitoring have

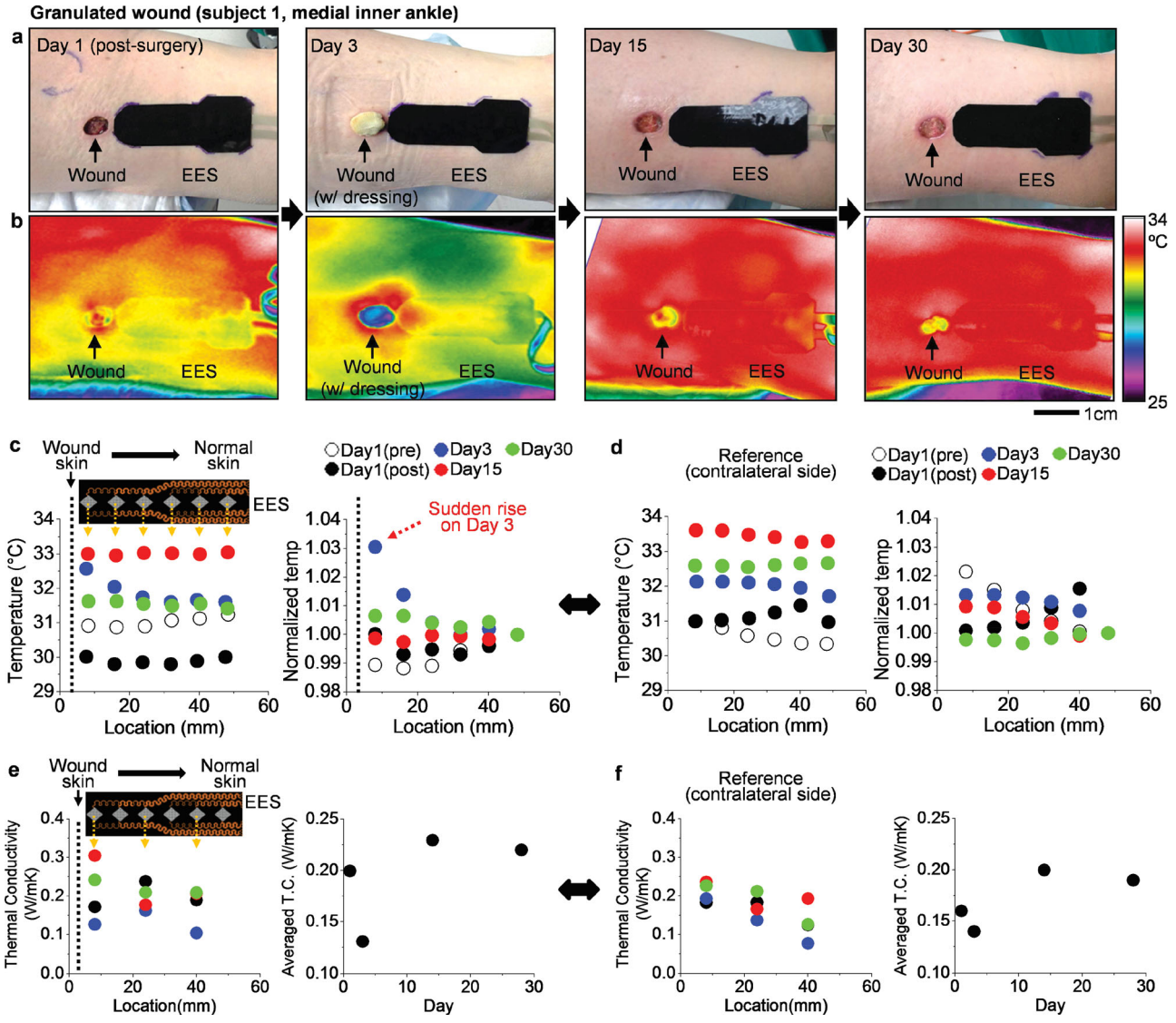

Figure 5. Quantitative monitoring of a granulating wound with an EES. a) Representative photos of the wound with an EES from day 1 to day 30. b) Corresponding IR images of the temperature distribution associated with (a). c) Temperature distribution recorded with an EES (inset) over the course of one month after the surgery. The six sensors span a distance of 45 mm in lateral direction, starting near the wound site. d) Temperature distribution on a contralateral side. e) Thermal conductivity (T.C.) recorded with three sensors in an EES (inset). f) Thermal conductivity (T.C.) on a contralateral side as a control.

typically focused only on the effect of balancing the hydration level in wound healing,[1] dressing materials,[45] or as in vitro testing with simulated wound beds.[9]

One subject (Subject 3) had a long surgical incision with suturing (**Figure 6**), protected by a dressing for the first two post-surgical weeks (Figure 6a). IR thermography captured temperature change for comparison with data obtained with an EES (Figure 6b). Another subject (Subject 1) had a granulating wound, which showed elevated calor on day 3, but also temperature elevation on day 15 (Figure 6c), perhaps reflecting prolonged, more intense inflammation.[1,14,44] Temperature variation near the wound site was clearly and reproducibly distinguishable from the minimal variance of the contralateral, control body temperature (Figure 6d). In the sutured wound, the extended inflammation phase demonstrated stable thermal conductivity during a prolonged period and differed from the temperature pattern of the granulating wound (Figure 6e). Temperature and thermal conductivity change on the contralateral site are shown in Figure S21 (Supporting Information). Subject 2, also with a granulating wound, showed trends similar to those of Subject 1 (**Table 1** and Figure S22, Supporting Information).

3. Discussion

Stretchable, conformal, multifunctional electronic sensor systems enable quantitative physiological measurements relevant to cutaneous wound management. The devices offer material

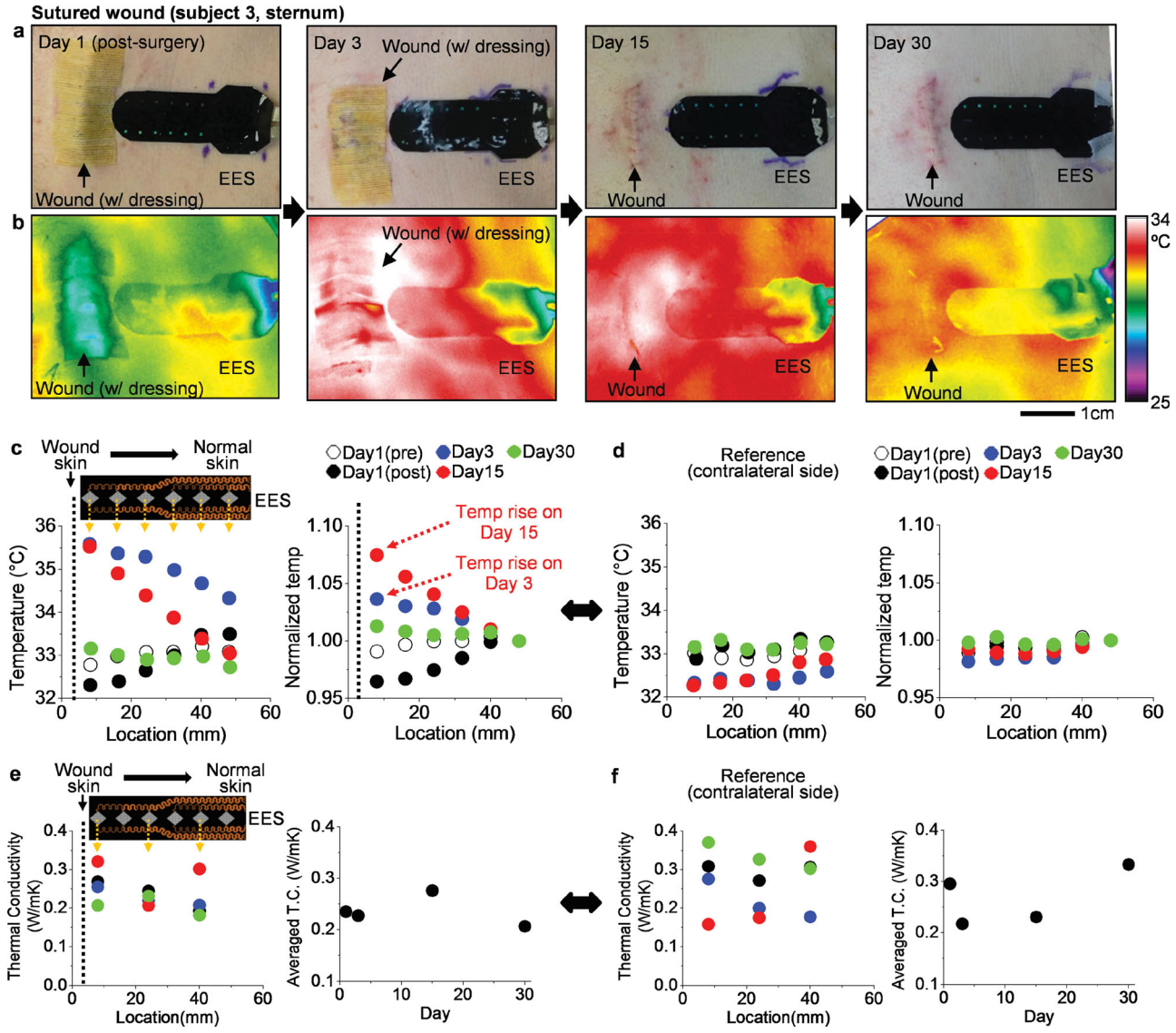

Figure 6. Quantitative management of sutured wound with an EES. a) Representative photos of the wound with an EES from day 1 to day 30. b) Corresponding IR images of the temperature distribution associated with (a). c) Temperature distribution recorded with an EES (inset) over the course of one month after the surgery. The six sensors span a distance of 45 mm in lateral direction, starting near the wound site. d) Temperature distribution on a contralateral side. e) Thermal conductivity (T.C.) recorded with three sensors in an EES (inset). f) Thermal conductivity (T.C.) on a contralateral side as a control.

Table 1. Summary of clinical study with three subjects.

	Subject 1	Subject 2	Subject 3
Wound type	Granulated	Granulated	Sutured
Age [years]	62	79	54
Sex	Male	Female	Male
Race	White, Caucasian	White, Caucasian	White, Caucasian
Site of lesion	Left medial inner ankle	Right shin	Sternum
Device contact[a)]	Conformal	Conformal	Conformal
Temperature rise	On day 3	On day 15	On days 3 and 15

[a)]Assessment by thermal conductivity measurement.

and mechanical properties that are well matched to human skin, allowing levels of integration of biotic and abiotic systems that are impossible with hard, flat, or merely flexible technologies. Biocompatible, ultra-soft layers of silicone completely encloses the electronics (effective moduli: ≈22 kPa, thickness: ≈500 μm) to provide enhanced wearability on hypersensitive wound tissues, simple procedures for disinfection, and re-use capabilities, all of which are required for use in a clinical setting. Multimodal functions, essential design criteria, and use in spatial mapping modes are supported by 3D FEM and FVM analysis.

Areas for future development include device configurations that allow direct lamination over the complex, textured geometry of a sutured wound site. Additional functions of interest include capabilities for measuring electromyograms, pH levels,

mechanical strain changes, and transepidermal water loss. Devices based on colorimetric readout thermochromic polymers could enable a cheap, portable monitoring without the use of sophisticated electronic devices and signal filtering/processing. Furthermore, incorporating wireless powering and transmission systems would deliver ideal mode for continuous wound management.

4. Conclusion

This article has introduced the use of a multifunctional, conformal EES in cutaneous wound management for patient applicability. Sets of micro-metal resistors demonstrated the multimodal measurement of high precision skin temperature, thermal conductivity in disinfected, re-use configuration and also showed the actuation function as micro-heaters. This class of technology is expanded further, with the support of 3D FEMs, to address unresolvable needs that include biocompatible, noninvasive, continuous monitoring of skin physiology in chronic wound management.

5. Experimental Section

Fabrication of an EES: The device processing used conventional microfabrication techniques (details in Note 2 and Figures S2 and S3, Supporting Information). A carrier substrate was prepared by spin coating thin layers of polydimethylsiloxane (PDMS; 10 μm in thickness, Dow Corning, USA) and polyimide (PI; 1.2 μm in thickness, Sigma-Aldrich, USA) on a 3-in. silicon wafer. Electron beam evaporation formed 3-μm-thick layers of Cu on the substrate. Photolithography and etching defined the fractal and FS traces. A water-soluble tape (3 M, USA) retrieved the completed patterns from the carrier wafer, for subsequent transfer and covalent bonding onto a black silicone membrane (Ecoflex, Smooth-On, USA). To provide electrical isolation for clinical use, a 5-μm-thick layer of silicone was coated on the top of patterns. For data acquisition, a flexible, anisotropic ribbon cable made electrical contact to the connection pads.

Biaxial Stretching and Imaging: Biaxial mechanical stretching of a fractal sensing component of an EES involved mounting onto a home-made plate with circular opening above an air chamber. Connecting the chamber to an external pump allowed controlled adjustment of biaxial strain induced by inflation. Three dimensional, micro X-ray tomography (Xradia, USA) was used to image microscale behaviors of the fractal traces (details in Supplementary Note 3, Supporting Information).

Clinical Study on Patients: All experiments on patients were conducted under a protocol (number: STU69718) approved by the Institutional Review Board, Northwestern University, Chicago, IL, USA. Prior to study entry, subjects signed written informed consents per adherence to Helsinki Guidelines. Research was carried out in a clinical exam room at the central Northwestern Medical Group Dermatology Clinic (676 North St. Clair Street, Suite 1600, Northwestern University, Feinberg School of Medicine, Chicago, IL, USA).

Supporting Information

Supporting Information is available from the Wiley Online Library or from the author.

Acknowledgements

W.-H.Y. thanks Jongwoo Lee, Dong Sup Lee, and Ohjin Kwon for help with the schematic illustration, material preparation and data analysis. This study was supported by the US Department of Energy, Division of Materials Sciences under Award No. DE-FG02–07ER46471 through the Materials Research Laboratory and Center for Microanalysis of Materials (DE-FG02–07ER46453) at the University of Illinois at Urbana-Champaign. This research utilized Core resources provided by the NIH-funded Northwestern University Skin Disease Research Center (NIAMS, P30AR057216). H.C. is a Howard Hughes Medical Institute International Student Research fellow. W.-H.Y. acknowledges the support of startup fund from the Virginia Commonwealth University. J.A.R. acknowledges a National Security Science and Engineering Faculty Fellowship.

Received: February 2, 2014
Published online: March 26, 2014

[1] T. R. Dargaville, B. L. Farrugia, J. A. Broadbent, S. Pace, Z. Upton, N. H. Voelcker, *Biosens. Bioelectron.* **2013**, *41*, 30.
[2] J. Panuncialman, S. Hammerman, P. Carson, V. Falanga, *J. Invest. Dermatol.* **2009**, *129*, S47.
[3] C. T. Hess, R. S. Kirsner, *Adv. Skin Wound Care* **2003**, *16*, 246.
[4] S. Lange-Asschenfeldt, A. Bob, D. Terhorst, M. Ulrich, J. Fluhr, G. Mendez, H. J. Roewert-Huber, E. Stockfleth, B. Lange-Asschenfeldt, *J. Biomed. Opt.* **2012**, *17*, 076016.
[5] N. J. Crane, E. A. Elster, *J. Biomed. Opt.* **2012**, *17*, 010902.
[6] T. Serena, Protease Activity Levels Associated with Healing Status of Chronic Wounds, http://www.systagenix.com/Promo/Product-Wall-2-EWMA-2012/posters/EP429.pdf, 2011.
[7] S. Guo, L. A. DiPietro, *J. Dent. Res.* **2010**, *89*, 219.
[8] G. Matzeu, M. Losacco, E. Parducci, A. Pucci, V. Dini, M. Romanelli, F. Di Francesco, *Proc. 37th Annu. Conf. IEEE IECON* **2011**, 3533.
[9] D. McColl, B. Cartlidge, P. Connolly, *Int. J. Surg.* **2007**, *5*, 316.
[10] D. H. Kim, N. S. Lu, R. Ma, Y. S. Kim, R. H. Kim, S. D. Wang, J. Wu, S. M. Won, H. Tao, A. Islam, K. J. Yu, T. I. Kim, R. Chowdhury, M. Ying, L. Z. Xu, M. Li, H. J. Chung, H. Keum, M. McCormick, P. Liu, Y. W. Zhang, F. G. Omenetto, Y. G. Huang, T. Coleman, J. A. Rogers, *Science* **2011**, *333*, 838.
[11] J. W. Jeong, W. H. Yeo, A. Akhtar, J. J. S. Norton, Y. J. Kwack, S. Li, S. Y. Jung, Y. W. Su, W. Lee, J. Xia, H. Y. Cheng, Y. G. Huang, W. S. Choi, T. Bretl, J. A. Rogers, *Adv. Mater.* **2013**, *25*, 6839.
[12] W. H. Yeo, Y. S. Kim, J. Lee, A. Ameen, L. K. Shi, M. Li, S. D. Wang, R. Ma, S. H. Jin, Z. Kang, Y. G. Huang, J. A. Rogers, *Adv. Mater.* **2013**, *25*, 2773.
[13] W. H. Yeo, R. C. Webb, W. Lee, S. Jung, J. A. Rogers, *Proc. SPIE* **2013**, *8725*, 1.
[14] T. Helfman, L. Ovington, V. Falanga, *Clin. Dermatol.* **1994**, *12*, 121.
[15] A. J. Singer, R. A. F. Clark, *New Engl. J. Med.* **1999**, *341*, 738.
[16] X. Huang, H. Y. Cheng, K. L. Chen, Y. L. Zhang, Y. H. Zhang, Y. H. Liu, C. Q. Zhu, S. C. Ouyang, G. W. Kong, C. J. Yu, Y. G. Huang, J. A. Rogers, *IEEE T. Bio-Med. Eng.* **2013**, *60*, 2848.
[17] X. Huang, W. H. Yeo, Y. H. Liu, J. A. Rogers, *Biointerphases* **2012**, *7*, 52.
[18] R. C. Webb, A. P. Bonifas, A. Behnaz, Y. H. Zhang, K. J. Yu, H. Y. Cheng, M. X. Shi, Z. G. Bian, Z. J. Liu, Y. S. Kim, W. H. Yeo, J. S. Park, J. Z. Song, Y. H. Li, Y. G. Huang, A. M. Gorbach, J. A. Rogers, *Nat. Mater.* **2013**, *12*, 1078.
[19] J. A. Fan, W.-H. Yeo, Y. Su, Y. Hattori, W. Lee, S. Jung, Y. Zhang, Z. Liu, H. Cheng, L. Falgout, M. Bajema, T. Coleman, D. Gregoire, R. Larson, Y. Huang, J. A. Rogers, *Nat. Commun.* **2013**, *5*, 3266.
[20] J. W. Jeong, M. K. Kim, H. Cheng, W. H. Yeo, X. Huang, Y. Liu, Y. Zhang, Y. Huang, J. A. Rogers, *Adv. Healthcare Mater.* **2013**, DOI: 10.1002/adhm.201300334.
[21] Y. M. Song, Y. Z. Xie, V. Malyarchuk, J. L. Xiao, I. Jung, K. J. Choi, Z. J. Liu, H. Park, C. F. Lu, R. H. Kim, R. Li, K. B. Crozier, Y. G. Huang, J. A. Rogers, *Nature* **2013**, *497*, 95.
[22] J. R. Davis, *Asm Specialty Handbook: Copper and Copper Alloys, ASM International* Materials Park, OH **2001**.

[23] W. F. Riley, L. D. Sturges, D. H. Morris, *Mechanics of Materials*, John Wiley & Sons, New York **1999**.
[24] Y. H. Zhang, S. Xu, H. R. Fu, J. Lee, J. Su, K. C. Hwang, J. A. Rogers, Y. G. Huang, *Soft Matter* **2013**, *9*, 8062.
[25] D. G. Cahill, *Rev. Sci. Instrum.* **1990**, *61*, 802.
[26] M. J. Assael, E. Charitidou, W. A. Wakeham, *Int. J. Thermophys.* **1989**, *10*, 793.
[27] S. R. Choi, D. Kim, *Rev. Sci. Instrum.* **2008**, *79*, 064901.
[28] R. Q. Gram, A. She, R. S. Craxton, D. R. Harding, *J. Appl. Phys.* **2012**, *112*, 033504.
[29] D. Haemmerich, P. F. Laeseke, *Int. J. Hyperthermia* **2005**, *21*, 755.
[30] D. H. Kim, S. D. Wang, H. Keum, R. Ghaffari, Y. S. Kim, H. Tao, B. Panilaitis, M. Li, Z. Kang, F. Omenetto, Y. G. Huang, J. A. Rogers, *Small* **2012**, *8*, 3263.
[31] C. J. Gannon, P. Cherukuri, B. I. Yakobson, L. Cognet, J. S. Kanzius, C. Kittrell, R. B. Weisman, M. Pasquali, H. K. Schmidt, R. E. Smalley, S. A. Curley, *Cancer-Am. Cancer Soc.* **2007**, *110*, 2654.
[32] T. Juang, D. Neuman, J. Schlorff, P. R. Stauffer, IEEE, in *Proc. 26th Ann. Int. Conf. IEE Eng. Med. Biol. Soc., Vols 1–7*, Vol. *26*, IEEE, New York **2004**, 3467.
[33] Y. S. Koo, A. E. Fathy, R. Kazemi, J. Phillips, IEEE, in: *2012 IEEE Antennas and Propagation Society International Symposium*, IEEE, New York **2012**.
[34] Infection Control Manual, https://practicegreenhealth.org/pubs/sharing/SHC_InfectionControlPolicy_7%2010CleaningofEquipment.pdf, Stanford Hospital and Clinics **2010**.
[35] G. McDonnell, A. D. Russell, *Clin. Microbiol. Rev.* **1999**, *12*, 147.
[36] Guideline for Disinfection and Sterilization in Healthcare Facilities, http://www.cdc.gov/hicpac/pdf/guidelines/Disinfection_Nov_2008.pdf, Disease Control Prevention 2008.
[37] J. M. Karp, R. Langer, *Nature* **2011**, *477*, 42.
[38] M. K. Kwak, H. E. Jeong, K. Y. Suh, *Adv. Mater.* **2011**, *23*, 3949.
[39] M. K. Kwak, C. Pang, H. E. Jeong, H. N. Kim, H. Yoon, H. S. Jung, K. Y. Suh, *Adv. Funct. Mater.* **2011**, *21*, 3606.
[40] B. Laulicht, R. Langer, J. M. Karp, *Proc. Natl. Acad. Sci. U.S.A.* **2012**, *109*, 18803.
[41] Y. J. Choi, S. Chae, J. H. Kim, K. F. Barald, J. Y. Park, S. H. Lee, *Sci. Rep.* **2013**, *3*, 1921.
[42] H. C. Jung, J. H. Moon, D. H. Baek, J. H. Lee, Y. Y. Choi, J. S. Hong, S. H. Lee, *IEEE T. Bio-Med. Eng.* **2012**, *59*, 1472.
[43] S. M. Lee, J. H. Kim, H. J. Byeon, Y. Y. Choi, K. S. Park, S. H. Lee, *J. Neural Eng.* **2013**, *10*, 036006.
[44] C. P. Pan, Y. H. Shi, K. Amin, C. S. Greenberg, Z. Haroon, G. W. Faris, *Biomed. Opt. Express* **2010**, *1*, 285.
[45] D. Queen, H. Orsted, H. Sanada, G. Sussman, *Int. Wound J.* **2004**, *1*, 59.

